Published in final edited form as:
Biomaterials. 2013 July ; 34(21): 5117–5127. doi:10.1016/j.biomaterials.2013.03.086.

The influence of matrix properties on growth and morphogenesis of human pancreatic ductal epithelial cells in 3D

Asad Raza, **Chang Seok Ki**, and **Chien-Chi Lin***
Department of Biomedical Engineering, Purdue School of Engineering and Technology, Indiana University-Purdue University at Indianapolis, Indianapolis, IN. 46202, USA

Abstract

A highly tunable synthetic biomimetic hydrogel platform was developed to study the growth and morphogenesis of pancreatic ductal epithelial cells (PDEC) under the influence of a myriad of instructive cues. A PDEC line, PANC-1, was used as a model system to illustrate the importance of matrix compositions on cell fate determination. PANC-1 is an immortalized ductal epithelial cell line widely used in the study of pancreatic tumor cell behaviors. PANC-1 cells are also increasingly explored as a potential cell source for endocrine differentiation. Thus far, most studies related to PANC-1, among other PDEC lines, are performed on 2D culture surfaces. Here, we evaluated the effect of matrix compositions on PANC-1 cell growth and morphogenesis in 3D. Specifically, PANC-1 cells were encapsulated in PEG-based hydrogels prepared by step-growth thiol-ene photopolymerization. It was found that thiol-ene hydrogels provided a cytocompatible environment for encapsulation and 3D culture of PANC-1 cells. In contrast to a monolayer morphology on 2D culture surfaces, PANC-1 cells formed clusters in 3D thiol-ene hydrogels within 4 days of culture. After culturing for 10 days, however, the growth and structures of these clusters were significantly impacted by gel matrix properties, including sensitivity of the matrix to proteases, stiffness of the matrix, and ECM-mimetic motifs. The use of matrix metalloproteinase (MMP) sensitive linker or the immobilization of fibronectin-derived RGDS ligand in the matrix promoted PANC-1 cell growth and encouraged them to adopt ductal cyst-like structures. On the other hand, the encapsulated cells formed smaller and more compact aggregates in non-MMP responsive gels. The incorporation of laminin-derived YIGSR peptide did not enhance cell growth and caused the cells to form compact aggregates. Immobilized YIGSR also enhanced the expression of epithelial cell markers including β-catenin and E-cadherin. These studies have established PEG-peptide hydrogels formed by thiol-ene photo-click reaction as a suitable platform for studying and manipulating pancreatic epithelial cell growth and morphogenesis in 3D.

Keywords

Hydrogels; cell encapsulation; pancreatic cancer; thiol-ene chemistry; cell-material interactions

*To whom correspondence should be addressed Chien-Chi Lin, Ph.D. Assistant Professor Department of Biomedical Engineering Indiana University-Purdue University at Indianapolis Indianapolis, IN 46202 Phone: 317-274-0760 Fax: 317-278-2455 lincc@iupui.edu.

1. Introduction

Pancreatic ductal epithelial cells (PDEC) are, as the name suggests, exocrine cells derived from epithelium in the pancreatic duct system. PDEC lines, such as PANC-1 cells, are commonly used to study the molecular mechanisms of pancreatic ductal adenocarcinoma (PDAC), a lethal cancer responsible for nearly 38,000 deaths in the US in 2012 [1]. Tissue culture plastics (TCP) are routinely used for culturing and studying PDAC cells *in vitro*. On TCP, PDAC cells such as PANC-1 adopt squamous phenotype, a characteristic morphology shared by many epithelium cells. Using two dimensional (2D) culture platforms, researchers have identified important pathways in relation to intracellular signaling in PDEC. While 2D studies have been invaluable, it is difficult to recapitulate critical aspects of extracellular matrix (ECM) microenvironment in conventional TCP culture. Recent efforts have focused on developing matrix systems for studying migration, invasion and morphogenesis of PDEC *in vitro*. For example, Matrigel® or collagen based systems were used to study the roles of transforming growth factor β (TGFβ) [2, 3], matrix metalloproteinase (MMP) [4], epidermal growth factor receptor (EGFR) [5], Trefoil factor 1 (TFF1) [6], and hypoxia [7] on PANC-1 cell migration and invasion. In another example, Korc and colleagues developed a Matrigel/soft agar composite 3D gel system to study the growth stimulatory effects of TGFβ [8] and molecular cross-talks between EGFR, TGFβ, with Src in PDEC lines [9]. Currently, the studies of PDEC in 3D are mostly relying on biologically-derived matrices that not only have undefined and batch-dependent biochemical compositions but also have very limited tunability in gel biophysical properties such as stiffness and molecular transport.

In addition to being used as a cell model for PDAC studies, pancreatic exocrine cells, such as PANC-1, are increasingly used in efforts related to endocrine differentiation [10–15]. PANC-1 cells can be trans-differentiated into insulin-secreting cell clusters under a serum deprivation condition and with the use of appropriate soluble cues such as glucagon-like peptide 1 (GLP−1) [10, 11], FGF2 [12], and stem cell factor (SCF) [13]. For example, Hardikar *et al*. reported the formation of islet-like cell aggregates from PANC-1 cells under serum deprivation and in the presence of FGF2 [12]. Recently, Dubiel *et al*. developed a RGD-covered dextran surface to enhance cluster formation and insulin expression in PANC-1 cells [16]. While the aforementioned studies were all conducted on 2D surfaces, they have highlighted the importance of ECM microenvironment, including soluble factors and immobilized integrin ligands, on the differentiation of exocrine PANC-1 cells into endocrine islet-like clusters.

The study of PDEC and trans-differentiation of PANC-1 cells into islet-like clusters can benefit from a synthetic material platform capable of recapitulating critical aspects of an ECM microenvironment. Such biomimetic matrices facilitate the mechanistic understanding of PDEC behaviors in a more physiologically relevant and well-defined microenvironment. One synthetic material platform with the potential of achieving these goals is poly(ethylene glycol) or PEG-based hydrogels decorated with biomimetic motifs [17–21]. Many PEG hydrogel systems have been developed for studying epithelial cell behaviors [17, 21], as well as differentiation of progenitor cells into pseudo-islets [22, 23]. In addition to the highly permeable environment created by the hydrophilic and biologically inert PEG macromers, aspects of ECM microenvironment critical for regulating cellular processes can be recapitulated within these well-defined niches. For example, ligands for cell surface receptors can be immobilized with precisely controlled concentrations to elicit desired intracellular signaling [24–26]. With appropriate cross-linking methods, encapsulated cells are allowed to migrate through the hydrogel mesh, which permits the understanding of cell invasion and metastasis mechanisms [27–29]. Finally, matrix stiffness can be easily controlled, by adjusting network cross-linking density, to study mechanosensing in the encapsulated cells [30–33].

Among the vast variety of PEG hydrogel platforms, step-growth PEG-norbornene-peptide hydrogels offer properties ideal for creating a synthetic biomimetic niche for 3D culture of PANC-1 cells. In addition to their mild and rapid reaction kinetics, these gels have proven cytocompatibility for cells derived from mesenchymal or epithelial origins [34, 35]. Using flexible PEG macromers and protease-sensitive peptides as gel cross-linkers, matrix remodeling can be dictated by local cellular activity. In this contribution, we aim at establishing a synthetic biomimetic microenvironment for encapsulation of PANC-1 cells, from which to study their growth and morphogenesis in 3D. We fist evaluated the initial viability of PANC-1 cells in thiol-ene hydrogels cross-linked by different linkers. We further assessed PANC-1 cell growth and morphological changes with various degrees of cell-material interactions, including protease-mediated matrix cleavage and integrin receptor binding. Morphogenesis of the encapsulated cells was evaluated via detecting expression of characteristic markers in the mesenchymal and epithelial lineages.

2. Materials and methods

2.1 Materials

4-arm PEG-OH (5 kDa and 20 kDa) was procured from JenKem Technology USA. Fmoc-amino acids, Fmoc-Rink-amide MBHA resin, and peptide synthesis reagents (HOBt, HBTU) were acquired from Anaspec or Chempep Inc. CellTiter Glo® and AlamarBlue® reagents were purchased from Promega and AbD Serotec, respectively. Live/Dead staining kit for mammalian cells was acquired from Life Technologies Corp. HPLC grade acetonitrile and water were purchased from Fisher Scientific and VWR International, respectively. All other chemicals were purchased from Sigma-Aldrich unless otherwise noted.

2.2 PEG-tetra-norbornene (PEG4NB) synthesis

PEG-tetra-norbornene (PEG4NB) was synthesized by reacting PEG-OH with 5-norbornene-2-carboxylic acid [34]. Briefly, 4-arm PEG-OH was dried in a vacuum oven overnight and dissolved in anhydrous toluene. After removing toluene using a rotary evaporator, the dried 4-arm PEG was dissolved in anhydrous dichloromethane (DCM). In a round bottom flask, 5-norbornene-2-carboxylic acid (5 eq.) was activated by N,N'-dicyclohexlycarbodiimide (DCC, 2.5 eq.) in anhydrous DCM for at least 30 minutes at room temperature. The activated norbornene acid was filtered through a fritted funnel and added drop-wisely into the flask containing dried 4-arm PEG-OH, 4-(dimethylamino)pyridine (DMAP, 0.5 eq.), and pyridine (5 eq.) dissolved in DCM. All reactions were performed in an ice bath and under nitrogen. After overnight reaction, the product was filtered and washed with 5 wt% sodium bicarbonate and brine to remove unreacted norbornene acid. The product was then dried over sodium sulphate and precipitated in cold ethyl ether. The filtered product was re-dissolved in DCM and re-precipitated in cold ethyl ether to obtain the final product. The degree of functionalization (> 85%) was analyzed using proton NMR (Avance III 500 Brucker). The photoinitiator lithium arylphosphinate (LAP) was synthesized following a published protocol without modification [36].

2.3 Peptide synthesis and purification

All peptides (CGGYC, KCGPQGPAGQCK, KCGPQGIWGQCK, CGRGDS, and CGYIGSR) were synthesized and cleaved using a microwave peptide synthesizer (CEM Discover SPS) following standard solid phase peptide synthesis (SPPS) chemistry. Terminal cysteines were added for thiol-ene reactions. Peptide cleavage solution contained 95 % trifluoroacetic acid (TFA), 2.5% water, and 2.5% triisopropylsilane (TIS) in the presence of 5wt/v% phenol. Crude peptides were precipitated in cold ethyl ether, dried overnight and purified using preparative scale RP-HPLC (PerkinElmer Flexar System). All peptides were

purified to at least 90% purity and characterized by analytical RP-HPLC and mass spectrometry (Agilent Technologies). Purified peptides were lyophilized and stored in −20 °C. Prior to usage, the concentration of thiol groups on purified cysteine-containing peptides was quantified using Ellman's reagent (PIERCE) following manufacturer's protocol.

2.4 Hydrogel fabrication

Thiol-ene hydrogels were prepared by step-growth photopolymerization using PEG4NB with two different molecular weights (20 kDa or 5 kDa) and di-thiol crosslinkers, including dithiolthreitol (DTT), CGGYC, KCGPQGPAGQCK (MMP_{scrm}), and KCGPQGIWGQCK (MMP_{Linker}). Thiol-ene photopolymerization was initiated using 1 mM LAP (dissolved in PBS) as the photoinitiator. Prepolymer solution containing $PEG4NB_{20kDa}$ or $PEG4NB_{5kDa}$, cross-linker, and LAP was exposed to long-wave UV light (365 nm, 5 mW/cm^2) for 2 minutes (Figure 1A). For all hydrogels, a stoichiometric ratio between thiol and ene groups was maintained. Gel stiffness was measured by oscillatory rheometry (See Supporting Method).

2.5 Cell culture and encapsulation

PANC-1 cells (obtained from ATCC) were maintained in high glucose DMEM (HyClone) containing 10% fetal bovine serum (Gibco) and 1× Antibiotic-Antimycotic (Invitrogen, 100 U/mL penicillin, 100 μg/mL streptomycin and 250 ng/mL Fungizone). Cells were maintained in tissue culture plastic kept at 37 °C and 5% CO_2 and the culture media were refreshed every 2 to 3 days. Cell encapsulation was performed using a procedure similar to the gel fabrication method described earlier. Briefly, PANC-1 cells (at a cell density of 2×10^6 cells/mL) were suspended in pre-polymer solutions containing PEG macromer, cross-linker, integrin ligand CRGDS or GCYIGSR (for some experimental groups) and photoinitiator. The precursor solutions were exposed to UV light (365 nm, 5 mW/cm^2) for 2 minutes. Cell-laden hydrogels (25 μL) were maintained in identical cell culture conditions as described earlier on an orbital shaker.

2.6 Cell viability and morphology characterizations

Qualitative cell viability was determined using Live/Dead staining and confocal imaging. Cell-laden hydrogels were incubated in Live/Dead staining solution for 1 hour at room temperature with gentle shaking. Confocal images of the stained samples were obtained using Olympus Fluoview FV100 Laser Scanning Biological Microscope (IUPUI Nanoscale Imaging Center). Z-stack images (100 μm thick, 10 μm per slice) from three samples and at least four random views were acquired for live (staining green) and dead (staining red) cell counts. Cell viability was defined as the percentage of live cells over total cell counts in each sample. To monitor long term cell viability, cell-laden hydrogels were incubated in 500 μL of 10% AlamarBlue® reagent in culture medium for 4 hours. Following incubation, 200 μL of the media were transferred to a 96-well plate and the fluorescence generated was measured using a microplate reader (excitation: 560 nm, emission: 590 nm). Live/Dead staining was also used to visualize cell morphology at day 4, 7 and 10. Images from four samples and at least three random fields per sample were acquired for analysis. Live/Dead images from four samples and at least three random fields per sample were used for analyzing and PANC-1 cell morphology and aggregate diameters. Olympus Fluoview and ImageJ software were used for image analysis. PANC-1 cell morphology was categorized according the following: (I) Single cells, (II) Round cell aggregates, (III) Large irregular cell clusters, (IV) Clusters with short cellular processes, and (V) Cyst-like cell clusters. Total populations of each category were manually counted.

2.7 Wholemount immunostaining

β-catenin and F-actin expressions in PANC-1 cells were visualized by immunostaining 10-day post-encapsulation. Cell-laden hydrogels were fixed in 4% paraformaldehyde at room temperature for 45 minutes with gentle shaking. Samples were then rinsed with PBS and the encapsulated cells were permeabilized with 0.5% Triton X-100 in PBS at room temperature for 45 minutes with gentle shaking. Following permeabilization, samples were washed with PBS and blocked (5% BSA, 5% polyvinylpyrrolidone, and 20% fetal calf serum) overnight at 4 °C. Samples were sequentially incubated overnight at 4 °C in rabbit-anti-β catenin (Santa Cruz, 1:100), followed by incubation in FITC-labeled goat anti-rabbit IgG (Cell signaling, 1:1000) and rhodamine-phalloidin (Cytoskeleton, 1:100). The samples were rinsed with PBS, further stained with DAPI for 1 hour and washed with PBS. The fluorescence from encapsulated cells was visualized and imaged using confocal microscope.

2.8 Western blotting

Total proteins from encapsulated cells were extracted by first homogenizing the cell-laden hydrogels with a pellet mixer. The homogenized samples were lysed with cell lysis buffer containing 10 μL of Halt Protease inhibitor, 10 μL of EDTA, and 1mM of phenylmethylsulfonyl fluoride (PMSF) dissolved in 1 mL of RIPA Buffer. Total extract was collected by centrifugation at 8000 rpm for 10 minutes at 4 °C. Total protein extractions were concentrated in Centrifugal Filter Units (Millipore) at 14000 rpm for 20 minutes at 4 °C. Total protein concentrations were determined by Pierce BCA Protein Assay Kit (Thermo Scientific) following manufacturer protocol. Concentrated protein extracts were then subjected to SDS-PAGE using 10% Min-PROTEAN TGX Precast Gels (Bio-Rad). After separation, proteins were transferred on to 0.45 μm Immobilon-P PVDF transfer membrane (Millipore) using Bio-Rad Trans-Blot Turbo Transfer System. The blots were blocked overnight with 5% nonfat milk in TBST solution (1× PBS containing 0.5% Tween-20) at 4 °C. The blots were then sequentially incubated with diluted primary antibody, followed by incubation with HRP-conjugated secondary antibody (1 hour each) at room temperature. Primary antibodies used: Mouse anti-β-actin (Sigma, 1:1000); Rabbit anti-Vimentin (Cell Signaling, 1:1000); Rabbit anti-Snail (Cell Signaling, 1:500); Rabbit anti-β-catenin (Cell Signaling, 1:1000); Rabbit anti-E-cadherin (Cell Signaling, 1:1000). Secondary antibodies used: HRP-labeled goat anti-rabbit or anti-mouse IgG (Cell Signaling, 1:500 to 1:1000). The blots were washed with TBST solution for 1 hour and visualized using SuperSignal West Pico Detection Kit (Thermo Scientific) in a Fuji LAS 3000 imaging system. Analysis of band intensity was performed using ImageJ.

2.9 Statistical analysis

All experiments were conducted independently for three times and the results were presented as mean ± SD. Statistical analyses were performed using GraphPad Prism Software package. The cell viability and Western blotting band intensity analysis data were analyzed using a two-way analysis of variance (ANOVA) followed by a Bonferroni's post-hoc test. The cluster size distribution and cell morphology categorization data were analyzed using a one-way ANOVA followed by a Dunnett post-hoc test. Single, double, and triple asterisks represent $p < 0.05$, 0.001, and 0.0001, respectively. A p value < 0.05 was considered statistically significant.

3. Results

3.1 Cytocompatibility of thiol-ene hydrogels for PANC-1 cells

The ability to manipulate the growth and morphogenesis of pancreatic ductal epithelial cells (PDEC) in 3D represents a critical initial step towards mechanistic understanding of

intracellular signaling in these cells in a physiologically relevant microenvironment. Here, we first examined PANC-1 cell viability immediately following photoencapsulation (Figure 1). PANC-1 cells were encapsulated at 2×10^6 cell/mL in $PEG4NB_{20kDa}$ hydrogels (5 wt%, G' ~ 3 kPa) with different cross-linkers (Table 1). DTT, CGGYC, and MMP_{Scrm} are control linkers not sensitive to MMP-mediated cleavage, while MMP_{Linker} is susceptible to cleavage by various MMPs [37]. CGGYC was selected also because it can be cleaved by chymotrypsin, thus allowing rapid recovery of cell clusters formed within the gel matrices for further applications [35]. Cell encapsulation was achieved within 2 minutes of photopolymerization using a precursor solution containing macromer, cross-linker, cells at desired density, and photoinitiator LAP (Figure 1A). We found that varying cross-linker chemistry had no significant effect on initial viability in the encapsulated cells (Figures 1B & S1) and over 92% of the cells survived the photoencapsulation process as quantified by live/dead cell counts (Figure 1B). The effect of cross-linker type on initial cell viability was also assessed quantitatively by intracellular ATP measurements (Figure S1) and no significant difference was found in these conditions.

3.2 Effect of cross-linker on PANC-1 growth

We monitored the growth of encapsulated PANC-1 cells in $PEG4NB_{20kDa}$ hydrogels cross-linked by CGGYC, MMP_{Scrm}, or MMP_{Linker} using qualitative Live/Dead staining and quantitative AlamarBlue® metabolic activity assay. There was no visible difference in cell morphology for the first 7 days when comparing images obtained from gels with different cross-linkers (Figure 2A). Quantitative metabolic activity assay results also show no statistical difference in cell viability for the first 7 days (Figure 2B). At day 10, however, the encapsulated cells appeared to form larger clusters with different shapes (Figure 2A, day 10). Significant differences in cellular metabolic activities were also observed (Figure 2B). The use of MMP_{Linker} as the gel cross-linker supported the highest degree of cell growth, as demonstrated by the formation of large cell clusters (Figure 2A, bottom right image) and the highest degree of cellular metabolic activity (Figure 2B). Cyst-like structures (white arrow) formed only in MMP_{Linker} cross-linked hydrogels after 10-day culture.

3.3 Effect of Matrix stiffness and protease sensitivity

Next, we evaluated the effects of matrix stiffness and protease sensitivity on PANC-1 cell growth and morphogenesis in 3D. We encapsulated PANC-1 cells in thiol-ene gels formed by 5 wt% $PEG4NB_{5kDa}$ or $PEG4NB_{20kDa}$ and with DTT or MMP_{Linker} as the gel cross-linker. PEG4NB with different molecular weights were used to render the matrix with different stiffness while DTT and MMP_{Linker} were used to render gels with different cell-mediated matrix remodeling. The shear moduli (G') of $PEG4NB_{5kDa}$ and $PEG4NB_{20kDa}$ in the equilibrium swelling state were ~6 kPa and ~3 kPa, respectively (Figure S2). The moduli of these gels dropped roughly 50% after 10 days of *in vitro* culture but $PEG4NB_{5kDa}$ gels were still much stiffer than $PEG4NB_{20kDa}$ gels (data not shown). As shown in Figure 1B, 95 ± 2% of PANC-1 cells remained viable following photoencapsulation in 5 wt% $PEG4NB_{20kDa}$ hydrogels cross-linked by DTT. However, initial viability decreased to 77± 3% in $PEG4NB_{5kDa}$ gels (Figure S3). Even with the reduction in initial cell viability, PANC-1 cells in both gel systems still proliferated to form small cell clusters regardless of the molecular weight of PEG4NB macromer used (Figure 3A, top row). There was, however, small but statistically significant increase in PANC-1 cell metabolic activity after 7-day culture in DTT cross-linked gels in softer $PEG4NB_{20kDa}$ gels (Figure 3B). Note that the metabolic activity was normalized to day-1 in order to offset the variation in initial cell viability and allow us to compare cell growth under different matrix conditions. When the cells were cultured in hydrogels cross-linked by DTT, there was a ~38% increase in cell metabolic activity at day-10 when comparing $PEG4NB_{20kDa}$ gels to $PEG4NB_{5kDa}$ gels ($p < 0.001$). When encapsulated in MMP_{Linker}-cross-linked hydrogels, PANC-1 cells proliferated

to form larger clusters with vast difference in cell morphology (Figure 3A, bottom row). Cells encapsulated in stiffer $PEG4NB_{5kDa}$ hydrogels showed irregular cell shapes with extensive protrusions. On the other hand, cells encapsulated in softer $PEG4NB_{20kDa}$ gels appeared much larger and formed cyst-like structures. These cells also exhibited rapid increase in metabolic activity, especially in $PEG4NB_{20kDa}$ gels. Comparing cell growth in the two gel systems cross-linked by MMP_{Linker} (Figure 3C), an 82% increase in metabolic activity ($p < 0.001$) at day-10 was observed when the cells were cultured in softer $PEG4NB_{20kDa}$ gels.

3.4 Morphological variations of PANC-1 cells in 3D

Figure 4 shows the morphological variations of PANC-1 cells cultured in 3D thiol-ene hydrogels. We categorized all cell clusters into four groups based on Live/Dead staining images, including: (A) Small and compact cell aggregates; (B) Large and irregular cell clusters; (C) Small clusters with short cellular protrusions; and (D) Cyst-like cell clusters. Immunostaining was performed in hydrogels without ECM motifs to identify expression patterns in F-actin and β-catenin. F-actin was selected because it is a cytoskeletal protein that responds to matrix compositional changes while the staining of β-catenin revealed potential cell-cell interactions. Staining results revealed strong β-catenin expression in cell clusters with higher level of cell-cell interactions. It was also found that cell clusters with irregular shapes and protrusions had weaker β-catenin staining but stronger F-actin staining at the peripheral area of the clusters (Figure 4C). Lastly, the core of cyst-like clusters had no DAPI staining but expressed more β-catenin and F-actin.

3.4 Effect of integrin ligands

The results shown in Figures 1–4 were obtained from PEG4NB hydrogels without the incorporation of any ECM-mimetic motifs. To evaluate the influence of cell-adhesive motifs on PANC-1 cell growth and morphogenesis in 3D, we monitored PANC-1 cells in CGGYC cross-linked PEG4NB hydrogels immobilized with 1 or 2 mM of fibronectin-derived CGRGDS or laminin-derived CGYIGSR peptides. Cysteine residues were added in the sequence for thiol-ene reaction to immobilize these peptides in the hydrogels. The use of CGGYC linker allows the cells to adopt different morphologies under the influence of ECM-mimetic motifs while preventing excessive local matrix remodeling due to cell-secreted proteases (e.g., MMPs). As shown in Figure 5A, hydrogels incorporated with RGDS motifs promoted cell growth with increasing cyst-like cell structures. On the contrary, gels immobilized with YIGSR peptide restricted the degree of cell growth as the clusters formed appeared smaller and slightly more dead cells were observed. AlamarBlue assays showed slightly higher degree of cellular metabolic activity in RGDS-immobilized gels compared to `blank-slate' hydrogels (Figure 5B). On the other hand, the immobilization of YIGSR peptide at a higher peptide concentration (i.e., 2 mM) only slightly increased the viability of PANC-1 cells at day 10 (Figure 5C).

3.5 Effect of matrix compositions on morphology of PANC-1 cells

Figure 6A shows the categorization of cell aggregates based on their morphology in thiol-ene hydrogels with different matrix compositions. When PANC-1 cells were encapsulated in DTT cross-linked hydrogels using stiffer $PEG4NB_{5kDa}$ gels, approximately 28% of the total cell clusters (including single cells) counted appeared to remain single cell morphology (category I). Among the total clusters, ~58% was small and compact aggregates (category II). Decreasing gel stiffness by using $PEG4NB_{20kDa}$ (also DTT cross-linked) did not cause significant changes in the populations of cell clusters. In these gels, very few irregularly shaped (category IV) or cyst-like clusters (category V) were found. On the other hand, when MMP_{Linker} was used to cross-link PEG4NB hydrogels, the effect of gel stiffness caused high diversity in the distribution of cell clusters. More than 65% of clusters adopted irregular

shapes (category IV) in stiffer PEG4NB$_{5kDa}$ gels while less than 10% of the clusters fell in this category in softer PEG4NB$_{20kDa}$ gels. In softer PEG4NB$_{20kDa}$ gels, cells also appeared to have the most diverse populations.

Figure 6B shows the influence of ECM-mimetic motifs (RGDS or YIGSR) on the population of cell aggregates within PEG4NB$_{20kDa}$ hydrogels cross-linked by CGGYC peptide linker. Notably, when fibronectin-derived RGDS or laminin-derived YIGSR was incorporated in the gel matrix, the most populated cell clusters were still compact and small aggregates (category II) as compared to gels without any ECM motif. However, the use of RGDS motif increased the percentage of cell clusters adopting irregular shape (categories IV) in 1 mM RGDS-immobilized gels and cyst-like structures (categories V) in 2 mM RGDS-immobilized gels. This trend was not observed in YIGSR-immobilized gels.

3.7 Size distribution of PANC-1 cell aggregates

Table 2 and Figure S4A show the size distribution of PANC-1 cell aggregates formed in thiol-ene hydrogels using gel formulations outlined in Figure 3. For both DTT and MMP$_{Linker}$ linkers, increasing matrix stiffness resulted in decreased average aggregate diameters. On the other hand, clusters formed in MMP$_{Linker}$ cross-linked hydrogels appeared to be larger in size compared to in DTT cross-linked gels. Table 3 and Figure S4B show the size distribution of PANC-1 cell aggregates formed in thiol-ene hydrogels using gel formulations outlined in Figure 5. The immobilization of RGDS ligand resulted in significant increase in average diameters of PANC-1 cell clusters from 58.5 ± 2.9 μm to 71.6 ± 2.3 μm. On the contrary, immobilization of YIGSR ligand slightly reduced the average diameters of PANC-1 cell clusters (56.5 ± 1.3 μm and 52.3 ± 1.1 μm for 1 mM and 2 mM YIGSR, respectively).

3.8 Expression of mesenchymal and epithelial cell markers

Figure 7A shows the expression of key epithelial and mesenchymal protein markers in encapsulated PANC-1 cells detected by Western blotting 10 days post-encapsulation. Vimentin and Snail were used as mesenchymal markers while β-catenin and E-cadherin were employed as markers for epithelial cell-cell interactions. β-actin was used as loading control. Figure 7 also shows the results of the corresponding band intensity analysis (normalized to β-actin bands). It was found that matrix compositions affected the expression of these protein markers to various degrees. As shown on the left column of Figure 7A and Figure 7B, PANC-1 cells in both CGGYC and MMP$_{Scrm}$ cross-linked hydrogels expressed significantly higher levels of Vimentin compared to cells encapsulated in MMP$_{Linker}$ cross-linked gels ($p < 0.01$). On the other hand, β-catenin and E-cadherin were highly expressed in cells encapsulated in MMP$_{Linker}$ cross-linked gels ($p < 0.001$) compared to in CGGYC or MMP$_{Scrm}$ cross-linked gels. No significant difference was found in Snail expression level in these gels.

The blotting results shown in the middle column of Figure 7A and relative band intensity analysis results shown in Figure 7C represent the influence of matrix stiffness and protease sensitivity on protein expression in the encapsulated PANC-1 cells. Higher levels of Vimentin and Snail expression and lower levels of β-catenin and E-cadherin were observed in cells encapsulated in stiffer PEG4NB$_{5kDa}$ gels or in gels without protease sensitivity (e.g, DTT cross-linked gels) ($p < 0.0001$). PANC-1 cells in softer PEG4NB$_{20kDa}$ gels cross-linked by MMP$_{Linker}$ showed the highest levels of epithelial markers (β-catenin and E-cadherin) and the lowest levels of mesenchymal markers (Vimentin and Snail).

Finally, the expressions of these protein markers were also analyzed in hydrogels incorporated with ECM-mimetic motifs (right column in Figure 7A, and Figure 7D). The

immobilization of RGDS or YIGSR ligands did not alter the expression patterns of Vimentin and Snail in the encapsulated PANC-1 cells. Further, the incorporation of RGDS ligand only slightly enhanced the expression of E-cadherin in the encapsulated PANC-1 cells (not statistically significant). The presence of immobilized YIGSR, however, significantly increased the expression of epithelial markers β-catenin ($p < 0.05$ and $p < 0.0001$ for 1 mM and 2 mM YIGSR, respectively) and E-cadherin ($p < 0.001$ for both 1 mM and 2 mM YIGSR) when compared to blank-slate PEG4NB hydrogels.

4. Discussion

Prior efforts on 3D culture of PDEC have largely focused on the use of biological matrices such as Matrigel®. While inherently bioactive, the biochemical compositions of these matrices are not meticulously controlled and may vary from batch to batch. Further, when using these purely biological matrices, experimenters are provided with minimal control over parameters critical in cellular mechanosensing, such as stiffness. We reasoned that biomimetic thiol-ene hydrogels could provide highly tunable properties for controlling the growth and morphogenesis of PDEC in 3D. In this work, we encapsulated PANC-1 cells, an immortalized PDEC line, in thiol-ene hydrogels with user-defined matrix properties, including cross-linker chemistry, matrix stiffness, and cell-material interactions. We chose PANC-1 cells not only because they are commonly used to study molecular signaling in pancreatic cancer cells [5, 7, 38, 39], but also because they can be trans-differentiated into islet-like clusters for the treatment of diabetes [10–14, 16].

Results from Figures 1B and S1 demonstrated high cytocompatibility of thiol-ene photochemistry for in situ encapsulation of PANC-1 cells. We used Live/Dead staining images to reveal live (stained with calcein-AM for intracellular esterase activity) and dead PANC-1 cells (stained with ethidium homodimer-1 due to loss of cell membrane integrity) in gels with different compositions. We also quantified cell viability by ATP assay, which correlates directly to the number of metabolically active cells following photo-encapsulation. Since all gels used in Figure 1B contained no biomimetic motif (e.g., integrin ligands), the high viability of PANC-1 cells in all thiol-ene hydrogels tested could be attributed to the high cytocompatibility of the thiolene photochemistry. Even without the presence of any cell surface receptor ligand, PANC-1 cells were able to proliferate into clusters with strong cell-cell interactions (Figures 2A, 3A, 4) and increasing metabolic activity (Figures 2B, 3B, 3C) as time. In addition, cell cluster morphology was affected by hydrogel formulation. For example, PANC-1 cells encapsulated in softer hydrogels cross-linked with MMP_{Linker} formed large cyst-like structures (Figures 2A, 3A, and 4D) that were rarely seen in other non-MMP sensitive gels (i.e., DTT, CGGYC, or MMP_{Scrm} cross-linked gels). The high MMP sensitivity of MMP_{Linker} cross-linked gels afforded the highest degree of PANC-1 cell growth in 3D after 10-day *in vitro* culture (Figure 2B), likely due to enhanced local matrix remodeling by the cell-secreted MMPs. On the other hand, cells in non-MMP sensitive gels formed smaller and more compact aggregates (Figure 2A left and middle columns and Figure 3A top row). No difference in cell morphology (Figure 2A) and phenotype (Figures 7A, 7B) was found between cells encapsulated in CGGYC or MMP_{Scrm} peptide cross-linked gels, suggesting that PANC-1 cells did not actively remodel these matrices.

The increased expression of epithelial cell markers (e.g., β-catenin and E-cadherin) and decreased expression of mesenchymal cell markers (e.g., Vimentin) in cells encapsulated in MMP_{Linker} cross-linked hydrogels reflected the profound impact of matrix properties on PANC-1 cell morphogenesis in 3D (Figures 7A and 7B). The ability of PANC-1 cells to remodel their local matrix resulted in high percentages of cell clusters adopting irregular shapes or cyst-like structures (Figures 4C, 4D, 6A). On the other hand, when cells were

encapsulated in MMP_{Scrm} cross-linked gels, the proliferation appeared to be slower (Figure 2B) and the cells expressed lower level of epithelial cell markers (Figure 7B). While the use of MMP-sensitive linker encouraged cell growth and morphogenesis, we found that a higher degree of cell growth was also obtained using certain peptide linker not sensitive to MMPs, such as CGGYC (Figure 2B). When PANC-1 cells were encapsulated in CGGYC cross-linked gels, smaller but abundant cell clusters formed after 10-day culture (Figure 2A, left column). The growth supporting role of CGGYC cross-linked hydrogels might be a result caused by chymotrypsin-mediated matrix cleavage. It is possible that the encapsulated PANC-1 cells secreted chymotrypsin, a pancreatic exocrine enzyme, to cleave CGGY↓C and create a favorable environment for cell growth. However, we are not aware of any literature supporting this possibility. The enhanced cell growth in the CGGYC cross-linked gels might be a result of enhanced gel degradation due to the hydrolysis of ester bonds in PEG4NB macromer. We have shown that the hydrolytic degradation rate of thiol-ene hydrogels could be tuned by different linker chemistry [40]. We have also exploited this degradation mechanism to study the viability and spreading of human mesenchymal stem cells (hMSC), as well as spheroid formation in pancreatic MIN6 β-cells in 3D. When DTT was used as gel cross-linker, the resulting gels did not degrade as fast as CGGYC cross-linked gels and consequently reduced cell spreading and proliferation [41].

Results in Figure 2 shed lights on the influence of local matrix properties on regulating cellular responses to the extracellular signals. The gel matrices used in Figure 2, however, all have similar stiffness (G' ~ 3 kPa, Figure S2). Matrix stiffness has been shown to largely affect cell fate determination both on 2D surfaces and in 3D matrices. For example, tumor tissues are known to be stiffer than normal tissues [42] while the differentiation of stem cells are encouraged down osteogenic lineage in a stiffer microenvironment [43]. To delineate the profound impact of matrix stiffness on PANC-1 cell growth and morphogenesis, we designed thiol-ene gels with different stiffness (G' ~ 3 or 6 kPa) and cross-linked by linkers with different MMP sensitivity (DTT or MMP_{Linker}). The interplay between matrix stiffness and local matrix remodeling could be clearly seen in Figure 3A where cells responded to a minimal degree to the changes in matrix stiffness when they were encapsulated in non-MMP sensitive gels (i.e., DTT cross-linked). In these gels, PANC-1 cells remained their compact and round morphology (Figure 3A, top row), had comparable categorization in the diversity of cell clusters (Figure 6A), and exhibited no statistical differences in all epithelial and mesenchymal protein markers examined (Figure 7C, comparing 5 kDa-DTT and 20 kDa-DTT). On the other hand, stiffness played a crucial role in PANC-1 cell growth and morphogenesis in an MMP-sensitive microenvironment. There were striking variations in cell proliferation (Figure 3C), morphological differences (Figure 6A), and protein expression (Figure 7C). Even though the matrix was cross-linked by MMP-sensitive linkers, higher stiffness in these gels likely altered some intracellular signaling events that resulted in the restriction of PANC-1 cells to invade their local matrix.

Studies have shown that pancreatic epithelial cells, when cultured on 2D surfaces, express high levels of epithelial markers such as cytokeratin, β-catenin, E-cadherin, and express little to no mesenchymal markers such as Vimentin, Snail, Slug, and N-cadherin [38]. However, when cultured in three-dimensional matrices (e.g., collagen gels), PANC-1 cells have been shown to express high level of mesenchymal markers like Vimentin and Snail [4]. In our current study, PANC-1 cells in all gel formulations expressed high level of Vimentin, except in the softer gels cross-linked by $PEG4NB_{20kDa}$ and MMP_{Linker} (Figure 7). It is likely that PANC-1 cells encapsulated in $PEG4NB_{20kDa}$ gels cross-linked by MMP-sensitive peptides were able to extensively remodel their local environment and transition into a ductal phenotype. On the other hand, cells in gels with higher stiffness (e.g., using $PEG4NB_{5kDa}$ gels) or lacking cell-mediated matrix remodeling (e.g., using DTT, CGGYC, or MMP_{Scrm} cross-linkers) retained their mesenchymal phenotype in 3D, such as that

observed in collagen gels [4]. When cultured in 3D matrices, epithelial cells such as PANC-1 are likely to acquire an “epithelial-to-mesenchymal” transition (EMT), which is typically characterized by changes in cell morphology accompanied with decreased expression of epithelial markers (e.g., E-cadherin) and enhanced expression of mesenchymal markers (e.g., Vimentin) [44]. Parallel to prior reports on mammary [21] and kidney [17] epithelial cells, our studies indicated that pancreatic epithelial cells also adopt different phenotypes under the influence of matrix properties.

Results shown in Figures 1–4 were obtained from experiments using PEG hydrogels with varying protease sensitivity and stiffness without any ECM-mimetic motifs, which have been shown to affect cell fate determination by providing receptor-mediated signaling. The impact of ECM-mimetic ligands can be clearly seen in Figure 5A. Here, CGGYC peptide was used to cross-link $PEG4NB_{20kDa}$ hydrogels to permit cell growth without the influence of cell-mediated matrix remodeling. CGGYC was also selected because the gels could be eroded by user-supplemented chymotrypsin, thus allowing the recovery of cell clusters generated within the 3D matrix [35]. The sequences of these ECM-mimetic motifs had very different influence in PANC-1 cells cultured in 3D. While the effect of fibronectin-derived RGDS on promoting cell growth was observed as early as day-4 compared to `blank-slate' PEG hydrogels (when 2 mM of RGDS was immobilized, Figure 5B), laminin-derived YIGSR, even at a higher concentration of 2 mM, only slightly increased PANC-1 cell growth at day-10. PANC-1 cells formed larger cyst-like structures in RGDS-immobilized gels, while smaller clusters and slightly more dead cells were observed in YIGSR-immobilized gels (Figure 5A). These results were consistent with the morphological analysis using live/dead images containing cell clusters formed in these gels (Figure 6B). The analysis results also showed that the average diameters (Tables 2, 3) and the distribution of cell clusters with different sizes (Figure S4) were similar for cells in CGGYC cross-linked gels with 2 mM RGDS and in MMP_{Linker} cross-linked gels without RGDS motif. Interestingly, protein expression patterns were very different in these two gel systems (Figure 7). For example, β-catenin and E-cadherin were highly expressed in MMP_{Linker} cross-linked gels (without RGDS) while their expression were relatively lower in RGDS-immobilized gels cross-linked by CGGYC. In addition, the immobilization of YIGSR up-regulated the expression of epithelial cell markers, including β-catenin and E-cadherin (Figure 7D) without decreasing Vimentin and Snail expression, which was not the trend seen in MMP_{Linker} cross-linked gels (i.e., higher β-catenin & E-cadherin, lower Vimentin & Snail).

RGD peptide is known to bind to integrins (e.g., β_1 and β_3) and the binding enhances cell-matrix interactions and focal adhesion [45, 46]. RGD-integrin binding also induces expression of L1CAM in PDAC cells that augments cell migration and invasion [47]. Studies have shown that $\alpha_v\beta_3$ was up-regulated in invasive tumor cells and the down regulation of endogenous β_3 in PANC-1 cells significantly inhibited their growth [48]. On the other hand, laminin-derived YIGSR has been shown to inhibit growth and metastasis in many tumor cells [49–52]. YIGSR likely mimics the laminin-rich basement membrane microenvironment and restricts the invasiveness and motility of tumor cells, including PANC-1. While in this study the immobilization of YIGSR did not decrease Vimentin expression in the encapsulated PANC-1 cells, it did significantly enhanced the expression of β-catenin and E-cadherin, both of which are found in the adherens junctions is cells with extensive cell-cell interactions. The increased expression of these epithelial markers also indicated a potential dedifferentiation of PANC-1 cells [53, 54]. While enhanced expression of β-catenin and E-cadherin were also observed in cells encapsulated in MMP_{Linker} cross-linked gels (Figure 7B), these cells showed the most diverse cluster morphology (Figure 6A) that had little resemblance to endocrine cell clusters. On the other hand, PANC-1 cells encapsulated in YIGSR-immobilized gels formed smaller and more compact, and potentially

islet-like, clusters (Table 3 and Figure S4). The influences of RGD and YIGSR on tumor cell phenotypes have been studied in many epithelial cells in PEG-based hydrogels [17, 21]. To our knowledge, however, the influence of YIGSR on the formation of compact cell clusters (Figure 5A) and up-regulation of epithelial marker expression (Figure 7D) in pancreatic epithelial cells cultured in 3D has not been reported. The current understanding in PDEC growth, morphological changes, and protein expression in tunable synthetic biomimetic matrices will benefit future investigations on controlling PANC-1 cell trans-differentiation towards an endocrine lineage.

5. Conclusion

In summary, we have established a highly tunable synthetic biomimetic material platform for studying the growth and morphogenesis of pancreatic epithelial cells in 3D. Based on a cytocompatible thiol-ene photochemistry, our material system was easily tuned to render the otherwise inert PEG environment responsive to cellular activity. The growth and morphological changes in PANC-1 cells were affected by macromer molecular weight (or gel stiffness), cross-linker chemistry, and cell-matrix interaction. While PANC-1 cells formed large cyst-like structure in MMP-sensitive or RGDS-immobilized gels, they were more compact and adopt epithelial cell phenotype in non-MMP sensitive or YIGSR-immobilized gels. This hydrogel platform offers a highly controllable microenvironment not only for studying pancreatic tumor cell behaviors in 3D, but also for trans-differentiation of PANC-1 cells into pseudo-islets that may benefit the treatment of diabetes.

Supplementary Material

Refer to Web version on PubMed Central for supplementary material.

Acknowledgments

This project was funded by the NIH (R21EB013717), IUPUI Department of Biomedical Engineering (Faculty Start-up fund), and Indiana Diabetes Research Center (Pilot & Feasibility Grant). The authors thank Dr. Hiroki Yokota and Nancy Tanjung for their technical assistance in Western blotting, as well as Dr. Murray Korc for discussion in pancreatic cancer cell biology.

References

[1]. National Cancer Institute. http://www.cancer.gov/cancertopics/types/pancreatic

[2]. Kitaura Y, Chikazawa N, Tasaka T, Nakano K, Tanaka M, Onishi H, et al. Transforming growth factor beta 1 contributes to the invasiveness of pancreatic ductal adenocarcinoma cells through the regulation of CD24 expression. Pancreas. 2011; 40:1034–42. [PubMed: 21697762]

[3]. Shields MA, Dangi-Garimella S, Redig AJ, Munshi HG. Biochemical role of the collagen-rich tumour microenvironment in pancreatic cancer progression. Biochem J. 2012; 441:541–52. [PubMed: 22187935]

[4]. Shields MA, Dangi-Garimella S, Krantz SB, Bentrem DJ, Munshi HG. Pancreatic cancer cells respond to type I collagen by inducing snail expression to promote membrane type 1 matrix metalloproteinase-dependent collagen invasion. J Biol Chem. 2011; 286:10495–504. [PubMed: 21288898]

[5]. Binker MG, Binker-Cosen AA, Richards D, Oliver B, Cosen-Binker LI. EGF promotes invasion by PANC-1 cells through Racl/ROS-dependent secretion and activation of MMP-2. Biochem Biophys Res Commun. 2009; 379:445–50. [PubMed: 19116140]

[6]. Arumugam T, Brandt W, Ramachandran V, Moore TT, Wang HM, May FE, et al. Trefoil factor 1 stimulates both pancreatic cancer and stellate cells and increases metastasis. Pancreas. 2011; 40:815–22. [PubMed: 21747314]

[7]. Binker MG, Binker-Cosen AA, Richards D, Gaisano HY, de Cosen RH, Cosen-Binker LI. Hypoxia-reoxygenation increase invasiveness of PANC-1 cells through Rac1/MMP-2. Biochem Biophys Res Commun. 2010; 393:371–6. [PubMed: 20153729]

[8]. Sempere LF, Gunn JR, Korc M. A novel 3-dimensional culture system uncovers growth stimulatory actions by TGF beta in pancreatic cancer cells. Cancer Biol Ther. 2011; 12:198–207. [PubMed: 21613822]

[9]. Deharvengt S, Marmarelis M, Korc M. Concomitant targeting of EGF receptor, TGF-beta and Src points to a novel therapeutic approach in pancreatic cancer. PLos One. 2012; 7

[10]. Hui HX, Wright C, Perfetti R. Glucagon-like peptide 1 induces differentiation of islet duodenal homeobox-1-positive pancreatic ductal cells into insulin-secreting cells. Diabetes. 2001; 50:785–96. [PubMed: 11289043]

[11]. Bulotta A, Perfetti R, Hui HX, Boros LG. GLP-1 stimulates glucose-derived de novo fatty acid synthesis and chain elongation during cell differentiation and insulin release. J Lipid Res. 2003; 44:1559–65. [PubMed: 12777469]

[12]. Hardikar AA, Marcus-Samuels B, Geras-Raaka E, Raaka BM, Gershengorn MC. Human pancreatic precursor cells secrete FGF2 to stimulate clustering into hormone-expressing islet-like cell aggregates. Proc Natl Acad Sci U S A. 2003; 100:7117–22. [PubMed: 12799459]

[13]. Wu Y, Li J, Saleem S, Yee S-P, Hardikar AA, Wang R. c-Kit and stem cell factor regulate PANC-1 cell differentiation into insulin- and glucagon-producing cells. Lab Invest. 2010; 90:1373–84. [PubMed: 20531294]

[14]. Hiram-Bab S, Shapira Y, Gershengorn MC, Oron Y. Serum Deprivation Induces Glucose Response and Intercellular Coupling in Human Pancreatic Adenocarcinoma PANC-1 Cells. Pancreas. 2012; 41:238–44. [PubMed: 22129530]

[15]. Kordowich S, Mansouri A, Collombat P. Reprogramming into pancreatic endocrine cells based on developmental cues. Mol Cell Endocrinol. 2010; 323:62–9. [PubMed: 20025937]

[16]. Dubiel EA, Kuehn C, Wang RN, Vermette P. In vitro morphogenesis of PANC-1 cells into islet-like aggregates using RGD-covered dextran derivative surfaces. Colloids Surf B Biointerfaces. 2012; 89:117–25. [PubMed: 21962947]

[17]. Chung IM, Enemchukwu NO, Khaja SD, Murthy N, Mantalaris A, Garcia AJ. Bioadhesive hydrogel microenvironments to modulate epithelial morphogenesis. Biomaterials. 2008; 29:2637–45. [PubMed: 18377982]

[18]. Miller JS, Shen CJ, Legant WR, Baranski JD, Blakely BL, Chen CS. Bioactive hydrogels made from step-growth derived PEG-peptide macromers. Biomaterials. 2010; 31:3736–43. [PubMed: 20138664]

[19]. Shikanov A, Smith RM, Xu M, Woodruff TK, Shea LD. Hydrogel network design using multifunctional macromers to coordinate tissue maturation in ovarian follicle culture. Biomaterials. 2011; 32:2524–31. [PubMed: 21247629]

[20]. Phelps EA, Enemchukwu NO, Fiore VF, Sy JC, Murthy N, Sulchek TA, et al. Maleimide cross-linked bioactive PEG hydrogel exhibits improved reaction kinetics and cross-linking for cell encapsulation and in situ delivery. Adv Mater. 2012; 24:64–70. [PubMed: 22174081]

[21]. Weiss MS, Bernabe BP, Shikanov A, Bluver DA, Mui MD, Shin SJ, et al. The impact of adhesion peptides within hydrogels on the phenotype and signaling of normal and cancerous mammary epithelial cells. Biomaterials. 2012; 33:3548–59. [PubMed: 22341213]

[22]. Mason MN, Arnold CA, Mahoney MJ. Entrapped collagen type 1 promotes differentiation of embryonic pancreatic precursor cells into glucose-responsive beta-cells when cultured in three-dimensional PEG hydrogels. Tissue Eng Part A. 2009; 15:3799–808. [PubMed: 19537960]

[23]. Mason MN, Mahoney MJ. Selective beta-cell differentiation of dissociated Embryonic Pancreatic Precursor cells cultured in synthetic polyethylene glycol hydrogels. Tissue Eng Part A. 2009; 15:1343–52. [PubMed: 19072086]

[24]. Lin CC, Anseth KS. Cell-cell communication mimicry with poly(ethylene glycol) hydrogels for enhancing beta-cell function. Proc Natl Acad Sci U S A. 2011; 108:6380–5. [PubMed: 21464290]

[25]. Hern DL, Hubbell JA. Incorporation of adhesion peptides into nonadhesive hydrogels useful for tissue resurfacing. J Biomed Mater Res. 1998; 39:266–76. [PubMed: 9457557]

[26]. Moon JJ, Saik JE, Poche RA, Leslie-Barbick JE, Lee SH, Smith AA, et al. Biomimetic hydrogels with pro-angiogenic properties. Biomaterials. 2010; 31:3840–7. [PubMed: 20185173]

[27]. Schwartz MP, Fairbanks BD, Rogers RE, Rangarajan R, Zaman MH, Anseth KS. A synthetic strategy for mimicking the extracellular matrix provides new insight about tumor cell migration. Integr Biol. 2010; 2:32–40.

[28]. Patterson J, Hubbell JA. SPARC-derived protease substrates to enhance the plasmin sensitivity of molecularly engineered PEG hydrogels. Biomaterials. 2011; 32:1301–10. [PubMed: 21040970]

[29]. Turturro M, Christenson M, Larson J, Young DA, Brey EM, Papavasiliou G. MMP-Sensitive PEG diacrylate hydrogels with spatial variations in matrix properties stimulate directional vascular sprout formation. PLos One. 2013; 8:e58897. [PubMed: 23554954]

[30]. Kloxin AM, Kloxin CJ, Bowman CN, Anseth KS. Mechanical properties of cellularly responsive hydrogels and their experimental determination. Adv Mater. 2010; 22:3484–94. [PubMed: 20473984]

[31]. Tibbitt MW, Anseth KS. Hydrogels as extracellular matrix mimics for 3D cell culture. Biotechnol Bioeng. 2009; 103:655–63. [PubMed: 19472329]

[32]. Bryant SJ, Anseth KS, Lee DA, Bader DL. Crosslinking density influences the morphology of chondrocytes photoencapsulated in PEG hydrogels during the application of compressive strain. J Orthop Res. 2004; 22:1143–9. [PubMed: 15304291]

[33]. Appelman TP, Mizrahi J, Elisseeff JH, Seliktar D. The differential effect of scaffold composition and architecture on chondrocyte response to mechanical stimulation. Biomaterials. 2009; 30:518–25. [PubMed: 19000634]

[34]. Fairbanks BD, Schwartz MP, Halevi AE, Nuttelman CR, Bowman CN, Anseth KS. A versatile synthetic extracellular matrix mimic via thiol-norbornene photopolymerization. Adv Mater. 2009; 21:5005–10.

[35]. Lin CC, Raza A, Shih H. PEG hydrogels formed by thiol-ene photo-click chemistry and their effect on the formation and recovery of insulin-secreting cell spheroids. Biomaterials. 2011; 32:9685–95. [PubMed: 21924490]

[36]. Fairbanks BD, Schwartz MP, Bowman CN, Anseth KS. Photoinitiated polymerization of PEG-diacrylate with lithium phenyl-2,4,6-trimethylbenzoylphosphinate: polymerization rate and cytocompatibility. Biomaterials. 2009; 30:6702–7. [PubMed: 19783300]

[37]. Patterson J, Hubbell JA. Enhanced proteolytic degradation of molecularly engineered PEG hydrogels in response to MMP-1 and MMP-2. Biomaterials. 2010; 31:7836–45. [PubMed: 20667588]

[38]. Madden ME, Sarras MP. Morpholigical and biochemical characterization of a human pancreatic ductal cell line (PANC-1). Pancreas. 1988; 3:512–28. [PubMed: 3141917]

[39]. Zervos EE, Shafii AE, Haq M, Rosemurgy AS. Matrix metalloproteinase inhibition suppresses MMP-2 activity and activation of PANC-1 cells in vitro. J Surg Res. 1999; 84:162–7. [PubMed: 10357914]

[40]. Shih H, Lin CC. Cross-linking and degradation of step-growth hydrogels formed by thiol-ene photoclick chemistry. Biomacromolecules. 2012; 13:2003–12. [PubMed: 22708824]

[41]. Raza A, Lin CC. The influence of hydrogel degradation and functionality on cell survival and morphogenesis in 3D. Macromol Biosci. 2013 Under review.

[42]. Greenleaf JF, Fatemi M, Insana M. Selected methods for imaging elastic properties of biological tissues. Annu Rev Biomed Eng. 2003; 5:57–78. [PubMed: 12704084]

[43]. Engler AJ, Sen S, Sweeney HL, Discher DE. Matrix elasticity directs stem cell lineage specification. Cell. 2006; 126:677–89. [PubMed: 16923388]

[44]. Gavert N, Ben-Ze'ev A. Epithelial-mesenchymal transition and the invasive potential of tumors. Trends Mol Med. 2008; 14:199–209. [PubMed: 18406208]

[45]. Ruoslahti E. RGD and other recognition sequences for integrins. Annu Rev Cell Dev Biol. 1996; 12:697–715. [PubMed: 8970741]

[46]. Hersel U, Dahmen C, Kessler H. RGD modified polymers: biomaterials for stimulated cell adhesion and beyond. Biomaterials. 2003; 24:4385–415. [PubMed: 12922151]

[47]. Kiefel H, Bondong S, Pfeifer M, Schirmer U, Erbe-Hoffmann N, Schafer H, et al. EMT-associated up-regulation of L1CAM provides insights into L1CAM-mediated integrin signalling and NF-kappa B activation. Carcinogenesis. 2012; 33:1919–29. [PubMed: 22764136]

[48]. Desgrosellier JS, Barnes LA, Shields DJ, Huang M, Lau SK, Prevost N, et al. An integrin alpha(v)beta(3)-c-Src oncogenic unit promotes anchorage-independence and tumor progression. Nat Med. 2009; 15:1163–U89. [PubMed: 19734908]

[49]. Graf J, Iwamoto Y, Sasaki M, Martin GR, Kleinman HK, Robey FA, et al. Identification of an amino-acid-sequence in laminin mediateing cell attachment, chemotaxis, and receptor-binding. Cell. 1987; 48:989–96. [PubMed: 2951015]

[50]. Yamamura K, Kibbey MC, Jun SH, Kleinman HK. Effect of matrigel and laminin peptide YIGSR on tumor-growth and metasis. Semin Cancer Biol. 1993; 4:259–65. [PubMed: 8400148]

[51]. Iwamoto Y, Nomizu M, Yamada Y, Ito Y, Tanaka K, Sugioka Y. Inhibition of angiogenesis, tumour growth and experimental metastasis of human fibrosarcoma cells HT1080 by a multimeric form of the laminin sequence Tyr-IIe-Gly-Ser-Arg (YIGSR). Br J Cancer. 1996; 73:589–95. [PubMed: 8605091]

[52]. Yoshida N, Ishii E, Nomizu M, Yamada Y, Mohri S, Kinukawa N, et al. The laminin-derived peptide YIGSR (Tyr-Ile-Gly-Ser-Arg) inhibits human pre-B leukaemic cell growth and dissemination to organs in SCID mice. Br J Cancer. 1999; 80:1898–904. [PubMed: 10471037]

[53]. Qiao QL, Ramadani M, Gansauge S, Gansauge F, Leder G, Beger HG. Reduced membranous and ectopic cytoplasmic expression of beta-catenin correlate with cyclin D1 overexpression and poor prognosis in pancreatic cancer. Int J Cancer Suppl. 2001; 95:194–7.

[54]. Neureiter D, Zopf S, Dimmler A, Stintzing S, Hahn EG, Kirchner T, et al. Different capabilities of morphological pattern formation and its association with the expression of differentiation markers in a xenograft model of human pancreatic cancer cell lines. Pancreatology. 2005; 5:387–97. [PubMed: 15980667]

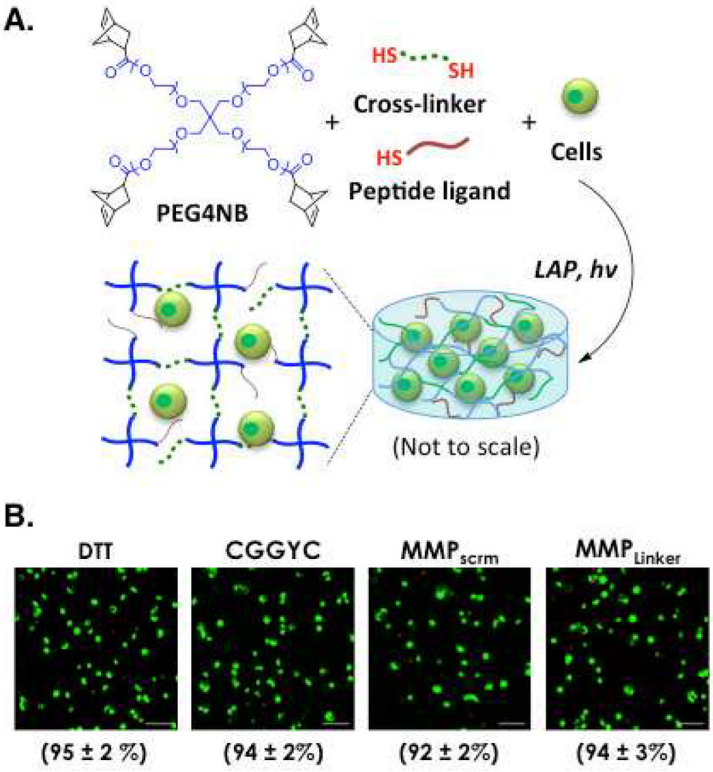

Figure 1.

(A) Schematic of thiol-ene photo-click reaction to form PANC-1 cell-laden PEG-based hydrogels. Gels are formed under UV light (365 nm, 5 mW/cm^2) exposure with 1 mM of lithium arylphosphinate (LAP) as the photoinitiator. 4-arm PEG-norbornene (PEG4NB, $f = 4$) and any multi-functional cross-linkers containing more than two thiol moieties (i.e., $f > 2$) are used to form step-growth hydrogels with an idealized network structure (image not to scale). (B) Representative confocal Z-stack images of PANC-1 cells stained with Live/Dead staining kit. Cells were encapsulated in 5 wt% PEG4NB$_{20kDa}$ gels with different cross-linkers. Numbers shown below each image represent the percentage of live cells over total cell count in each gel formation (Scales: 100 μm; N = 4, mean ± SD).

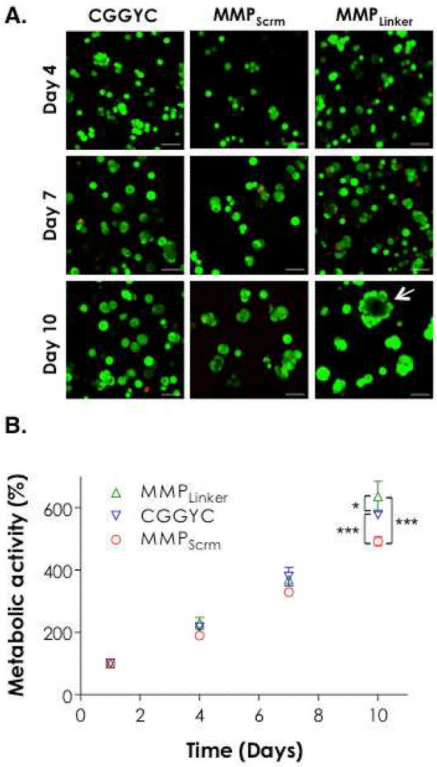

Figure 2.

Effect of cross-linker chemistry on PANC-1 cell growth and morphogenesis in 5 wt% $PEG4NB_{20kDa}$ hydrogels. (A) PANC-1 cell morphology visualized by Z-stack confocal microscope after Live/Dead staining at day 4, 7, and 10 (Scales: 100 μm). (B) Cell metabolic activity measured as a function of time by AlamarBlue® reagent. All readings were normalized to day-1 values in the respective group. Single and triple asterisks represent a p value of < 0.05 and < 0.0001, respectively.

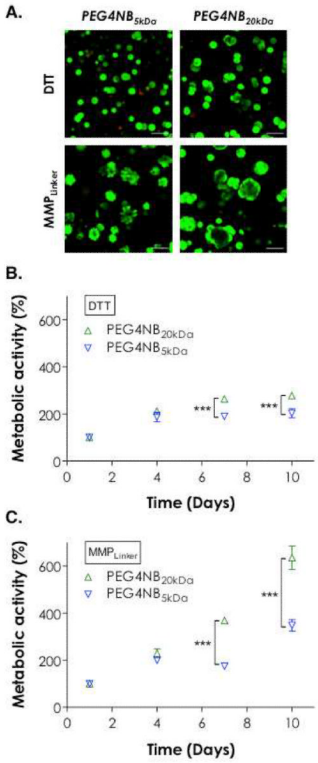

Figure 3.

Effect of PEG4NB molecular weight and cross-linker chemistry on PANC-1 cell morphogenesis. (A) Representative confocal Z-stack images of PANC-1 cells stained with Live/Dead staining kit 10 days post-encapsulation. Cells were encapsulated in 5 wt% $PEG4NB_{5kDa}$ or $PEG4NB_{20kDa}$ hydrogels cross-linked by DTT or MMP_{Linker} (Scales: 100 μm). (B) Effect of matrix stiffness on cell growth in DTT cross-linked gels. (C) Effect of matrix stiffness on cell growth in MMP_{Linker} cross-linked gels. Cell metabolic activity was measured by AlamarBlue® reagent and normalized to day-1 value in the respective group. Triple asterisks represent $p < 0.0001$.

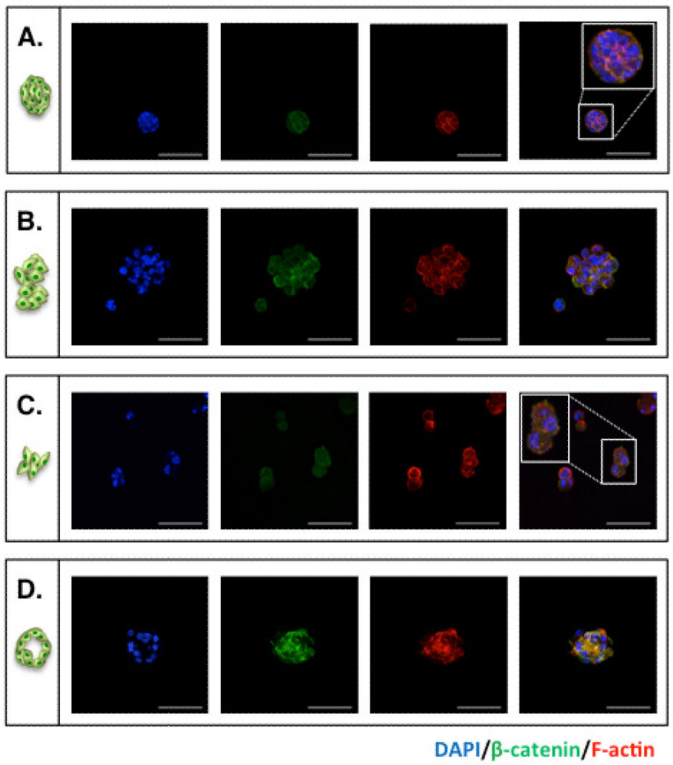

Figure 4.
Representative immunostaining images of PANC-1 cells encapsulated in PEG4NB hydrogels. At day 10 post-encapsulation, PANC-1 cells were stained using antibodies targeting β-catenin (green) and F-actin (red). Cell nuclei were counter-stained with DAPI (blue). (A) Single cells; (B) Small and compact cell aggregates; (C) Large and irregular cell clusters; (D) Small clusters with short cellular protrusions; and (E) Cyst-like cell clusters (Scales: 100 μm).

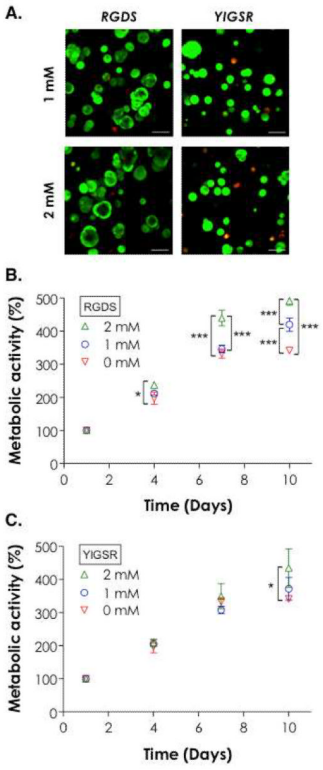

Figure 5.

Effect of ECM-mimetic motifs on PANC-1 cell growth and morphogenesis. (A) Representative confocal Z-stack images of PANC-1 cells stained with Live/Dead staining kit 10 days post-encapsulation. Cells were encapsulated in 5 wt% PEG4NB20kDa hydrogels cross-linked by CGGYC peptide and immobilized with 1 or 2 mM CGRGDS or CGYIGSR (Scales: 100 μm). (B) Effect of RGDS concentration on cell growth. (C) Effect of YIGSR on cell growth. Cell metabolic activity was measured by AlamarBlue® reagent and normalized to day-1 value in the respective group. Single and triple asterisks represent a p value of < 0.05 and < 0.0001, respectively.

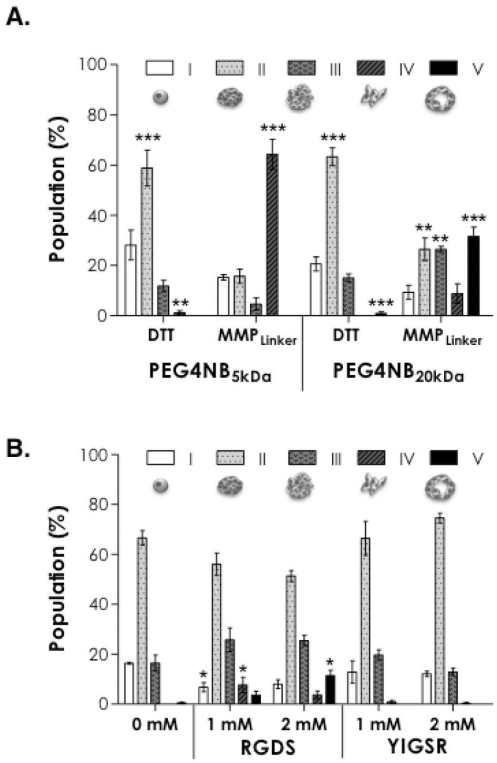

Figure 6.

Categorization of PANC-1 cell morphology in PEG4NB hydrogels with: (A) different PEG4NB molecular weights and cross-linkers, and (B) different ECM-mimetic motifs. Categories are: (I) Single cells; (II) Small and compact cell aggregates; (III) Large and irregular cell clusters; (IV) Small clusters with short cellular protrusions; and (V) Cyst-like cell clusters. Live/Dead staining images were used to analyze cell morphology at day-10 post-encapsulation (N = 4, mean ± SD). Control group used in statistical analysis for (A) was the population of category I in each gel formation. Control group used in statistical analysis for (B) was 0 mM ligand in each category. Single, double, and triple asterisks represent $p < 0.05$, < 0.001, and 0.0001, respectively.

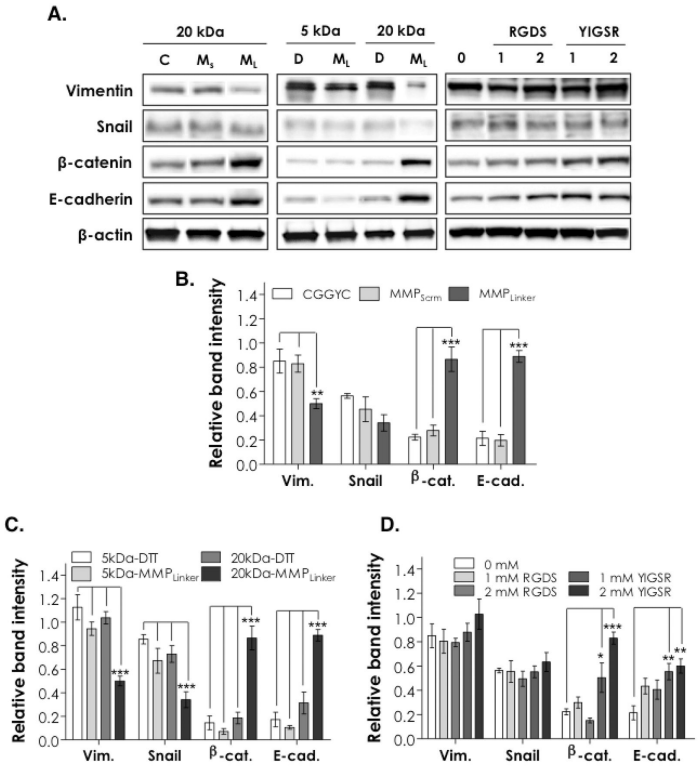

Figure 7.

(A) Western blotting for mesenchymal (Vimentin, and Snail) and epithelial (β-catenin and E-cadherin) lineage specific markers in PANC-1 cells 10 days post-encapsulation (C: CGGYC, M_S: MMP_{Scrm}, M_L: MMP_{Linker}). (B-D) Semi-quantitative analysis of protein band intensities (Vim: Vimentin, β-cat: β-catenin, E-cad: E-cadherin). Band intensities were obtained by ImageJ and normalized to that of β-actin in the respective group (N = 4, mean ± SD). Single, double, and triple asterisks represent a *p* value of < 0.05, < 0.001, and < 0.0001, respectively.

Table 1

Characteristics of the cross-linkers used to form thiol-ene hydrogels.

Label	Linker chemistry	Linker degradability	Gel degradability
DTT	Dithiothreitol	Non-cleavable	Hydrolytic *
CGGYC	CGGY[a]C	Chymotrypsin sensitive	Hydrolytic * & enzymatic
MMP_{scrm}	KCGPQGPAGQCK	Non-cleavable	Hydrolytic *
MMP_{Linker}	KCGPQG[b]IW[a]GQCK	MMPs & chymotrypsin sensitive	Hydrolytic * & enzymatic

DTT cross-linked gels had the slowest degradation rate [40].

[a] P1 positions for chymotrypsin-mediated cleavage

[b] P1 position for metalloproteinase (MMP)-mediated cleavage

* Hydrolytic degradation rate of hydrogels depends on the linker.

Table 2

Average diameters of PANC-1 cell clusters in thiol-ene hydrogels formed by $PEG4NB_{5kDa}$ or $PEG4NB_{20kDa}$ with different cross-linker chemistry (Mean ± SD).

PEG4NB MW (kDa)	Linker chemistry	Avg. diameter (μm)	n	*p* value
5	DTT	42.6 ± 0.8	345	*<0.0001*
	MMP_{Linker}	56.0 ± 1.2	236	
20	DTT	50.7 ± 1.2	256	*<0.0001*
	MMP_{Linker}	74.1 ± 2.7	158	

Table 3

Average diameters of PANC-1 cell clusters in thiol-ene hydrogels formed by 5 wt% $PEG4NB_{20kDa}$ cross-linked by CGGYC peptide and incorporated with different ECM-mimetic motifs (Mean ± SD).

ECM-mimetic motif	Cone. (mM)	Avg. diameter (μm)	n	*p* value
RGDS	0	58.5 ± 2.9	200	-
	1	66.2 ± 1.8	229	< 0.0001
	2	71.6 ± 2.3	192	< 0.0001
YIGSR	1	56.5 ± 1.3	195	> 0.05
	2	52.3 ± 1.1	226	> 0.05